Comparison of $^{10}B + {}^{6}Li$ and $^{10}B + {}^{7}Li$ elastic scattering: The role of ground state reorientation and breakup

A. T. Rudchik,[1] A. A. Rudchik,[1] O. O. Chepurnov,[1] K. W. Kemper,[2] N. Keeley,[3,*] K. Rusek,[4] E. I. Koshchy,[5] S. Kliczewski,[6,†] S. Yu. Mezhevych,[1] V. M. Pirnak,[1] O. A. Ponkratenko,[1] R. Siudak,[6] H. M. Maridi,[4] A. P. Ilyin,[1] B. V. Mishchenko,[1] Yu. M. Stepanenko,[1] V. V. Uleshchenko,[1] Yu. O. Shyrma,[1] K. A. Chercas,[1] and B. Zalewski[4]

[1]*Institute for Nuclear Research, Ukrainian National Academy of Sciences, Prospect Nauky 47, 03680 Kyiv, Ukraine*

[2]*Department of Physics, Florida State University, Tallahassee, Florida 32306, USA*

[3]*National Centre for Nuclear Research, ul. Andrzeja Sołtana 7, 05-400 Otwock, Poland*

[4]*Heavy Ion Laboratory, University of Warsaw, Pasteura 5A, 02-093 Warsaw, Poland*

[5]*Cyclotron Institute Texas A&M University, College Station, Texas 77843, USA*

[6]*Henryk Niewodniczański Institute of Nuclear Physics, Polish Academy of Sciences, ul. Radzikowskiego 152, 311-342 Kraków, Poland*

(Received 21 June 2022; accepted 12 July 2022; published 20 July 2022)

Angular distributions of the differential cross section for elastic scattering and $^{6}Li \rightarrow \alpha + d$ resonant breakup in the $^{10}B + {}^{6}Li$ system were measured in inverse kinematics with a 51-MeV ^{10}B beam. A comparison with existing data for the $^{10}B + {}^{7}Li$ system at the same incident ^{10}B energy revealed an important difference in the backward angle elastic scattering, with that for $^{10}B + {}^{6}Li$ being significantly larger in magnitude. A series of coupled channel and coupled discretized continuum channel calculations investigated the influence of ^{10}B and ^{7}Li ground state reorientation and breakup couplings on the elastic scattering. Elastic transfer of a ^{4}He and ^{3}He cluster between the ^{6}Li and ^{7}Li cores, respectively, was also investigated. Although a conclusive explanation of the observed difference in the backward angle elastic scattering between the two systems was not obtained, the elastic transfer mechanism could be definitively ruled out as a significant factor and there were indications that a difference in the effect of the breakup coupling may play a role even in these light systems. The ground state reorientation coupling in ^{7}Li, while exhibiting an interesting interference effect with the ^{10}B ground state reorientation, was also found to make a negligible contribution to the difference in backward angle elastic scattering.

DOI: 10.1103/PhysRevC.106.014615

I. INTRODUCTION

The present work continues an investigation into the influence on the elastic scattering in systems involving $1p$-shell nuclei of different reaction processes, such as inelastic excitations, including ground state reorientation and breakup, and possible one- and two-step nucleon and cluster transfers. Such studies can be challenging due to the large number of reaction channels potentially involved. In this work, elastic scattering and $^{6}Li \rightarrow \alpha + d$ resonant breakup angular distributions for the $^{10}B + {}^{6}Li$ system were measured in inverse kinematics with a 51-MeV ^{10}B beam and compared with existing data for the $^{10}B + {}^{7}Li$ system at the same incident ^{10}B energy [1]. Data for the $^{6}Li + {}^{10}B$ elastic scattering, measured in direct kinematics with a 30-MeV ^{6}Li beam, have previously been reported [2]. The center of mass energy, 18.74 MeV, matches very well with that of the present data, 19.14 MeV. However, the data reported here extend the angular range from $\theta_{\text{c.m.}} = 110^{\circ}$ to $\theta_{\text{c.m.}} = 168^{\circ}$ as well as including the nonresonant breakup.

The main goal of the present work is to compare the elastic scattering of the two systems $^{10}B + {}^{6}Li$ and $^{10}B + {}^{7}Li$ at the same incident ^{10}B energy ($E_{\text{c.m.}} = 19.14$ and 21.02 MeV, respectively). The ^{10}B nucleus has a large ground state quadrupole moment [3], which can have a significant influence on the elastic scattering via reorientation coupling effects; see, for example, Parks *et al.* [4]. In addition, ^{7}Li is significantly deformed, also demonstrating an important ground state reorientation coupling effect on the elastic scattering; see, e.g., Hnizdo *et al.* [5], whereas the ground state quadrupole moment of ^{6}Li is essentially zero [6], leading to an absence of reorientation coupling effects in ^{6}Li scattering. The difference of $\approx$1 MeV in breakup threshold between the two Li isotopes may also play a role in any differences between the elastic scattering of these systems, although with such a light partner nucleus as ^{10}B and at an energy well into the Fraunhofer scattering regime one would not expect it to have a major influence. Finally, in the $^{10}B + {}^{6}Li$ system elastic transfer of an α particle cluster between the two ^{6}Li cores can occur, although the spectroscopic amplitude for this overlap calculated within the translationally invariant shell model (TISM) is small [1], whereas in the $^{10}B + {}^{7}Li$ system the equivalent process involves transfer of a ^{3}He cluster and the TISM spectroscopic amplitudes for this overlap are

*Corresponding author: nicholas.keeley@ncbj.gov.pl
†Deceased.

significantly larger [1]. Nevertheless, the effect of this coupling on the $^{10}B + ^{7}Li$ elastic scattering at an incident ^{10}B energy of 51 MeV was found to be small in Ref. [1]. It is therefore not *a priori* obvious that there will be any significant difference between the elastic scattering of the two systems, and if such a difference does exist, what its root cause will be.

After a brief description of the experimental procedure and optical model fits to the elastic scattering data using standard Woods-Saxon volume potential forms, this paper falls naturally into two main parts. In the first part, the influence of ground state reorientation of both ^{10}B and ^{7}Li and elastic transfer of a ^{4}He or ^{3}He cluster between the ^{6}Li and ^{7}Li cores, respectively, is examined through a series of standard coupled channel (CC) fits and coupled reaction channel (CRC) calculations. The standard CC theory is the most appropriate for an analysis of the reorientation couplings. The second part investigates the influence of $^{6,7}Li$ breakup coupling effects on the elastic scattering via coupled discretized continuum channel (CDCC) calculations. Note that the CC analysis comprises *fits*, since the parameters of the diagonal optical model potentials used as input were adjusted to give the best description of the elastic scattering data, whereas the CDCC calculations are parameter free in the sense that none of the input parameters were adjusted to fit the $^{10}B + ^{6,7}Li$ data. This important difference between the two parts of the analysis should be borne in mind in what follows. The use of the CC fitting procedure enables the ^{10}B reorientation coupling, which cannot conveniently be included in the CDCC analysis, to be studied in isolation in a physically meaningful fashion.

II. EXPERIMENTAL PROCEDURE

Angular distributions for the $^{6}Li(^{10}B, X)$ reactions were measured at an incident ^{10}B energy of $E_{lab} = 51$ MeV using a ^{10}B beam provided by the U-200P cyclotron of the Heavy Ion Laboratory of the University of Warsaw. The beam energy spread on target was about 0.5%. A 900 $\mu g/cm^2$ thick self-supporting lithium foil enriched to 85% in ^{6}Li was used as a target. Reaction products with $Z = 3$–7 were detected using two types of $\Delta E - E$ telescopes: (1) both the ΔE and E stages consisted of solid state silicon detectors and (2) the ΔE stage consisted of a gas-filled ionization chamber while the E stage was a solid state silicon detector. The working gas in the ionization chamber was argon at a pressure such that the energy losses were equivalent to those of a 15-μm-thick silicon detector. The reaction products were well resolved in charge and mass. Data readout was via standard CAMAC electronics and the SMAN data acquisition system [7].

Typical energy spectra for the detection of ^{10}B and ^{6}Li ions measured with a telescope composed wholly of silicon detectors are shown in Figs. 1(a) and 1(b), respectively. These spectra were obtained after subtraction of background from multiparticle reactions. Peaks were fitted with symmetric Gaussian functions and the areas under the peaks of the ^{10}B and ^{6}Li spectra were used to extract cross sections at scattering angles $\theta_{c.m.}(^{10}B)$ and $\theta_{c.m.}(^{10}B) = 180^\circ - \theta_{c.m.}(^{6}Li)$, respectively. In this way, angular distributions for the $^{10}B + ^{6}Li$ elastic scattering as well as for inelastic scattering leading to the ^{10}B excitations could be determined over

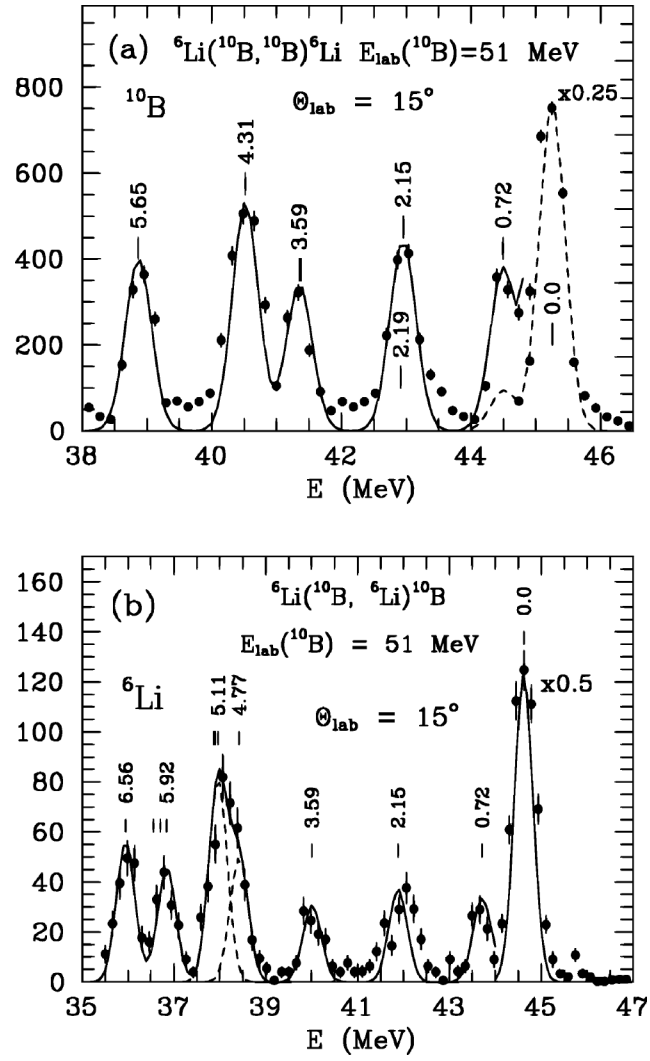

FIG. 1. Typical residual E spectra for detection of ^{10}B (a) and ^{6}Li (b) at an incident energy of $E_{lab}(^{10}B) = 51$ MeV after the subtraction of background from multiparticle reactions. The curves denote symmetric Gaussian fits to the peaks.

the whole angular range. For inelastic scattering leading to excitation of $\alpha + d$ resonant states of ^{6}Li data were obtained at forward angles only, from the spectra for detection of the ^{10}B. In this work, we present angular distributions for the elastic scattering and excitation of the resonant ^{6}Li states only. The elastic scattering angular distribution matches very well the data of Kemper *et al.* [2] taken in direct kinematics at an incident ^{6}Li energy of 30 MeV ($E_{c.m.} = 18.74$ MeV compared to $E_{c.m.} = 19.14$ MeV for the present data) in the angular range where they overlap, cf. the open and filled circles in Fig. 2.

III. DATA ANALYSIS

All calculations were performed using the code FRESCO [8] and all parameter searches were carried out with the SFRESCO package.

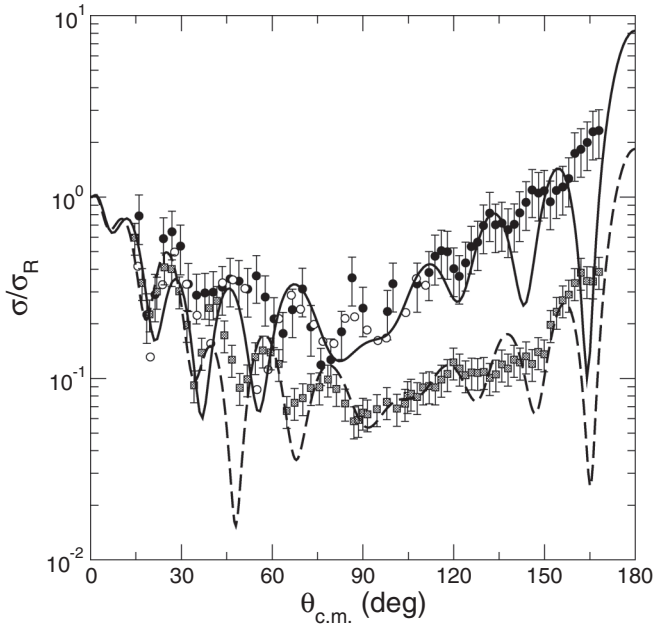

FIG. 2. Comparison of $^{10}B + {}^{6,7}Li$ elastic scattering data for an incident ^{10}B energy of 51 MeV. The filled circles denote the $^{10}B + {}^{6}Li$ data obtained in this work and the open circles those of Kemper *et al.* [2]. The $^{10}B + {}^{7}Li$ data of Rudchik *et al.* [1] are denoted by the shaded squares. The solid and dashed curves are the results of OM calculations with the $^{10}B + {}^{6}Li$ and $^{10}B + {}^{7}Li$ potential parameters listed in Table I, respectively.

A. Optical model fitting

The first stage of the analysis was to fit the data for both $^{10}B + {}^{6}Li$ and $^{10}B + {}^{7}Li$ elastic scattering using the optical model (OM). The potentials were of standard Woods-Saxon volume form, with the Coulomb potential being that for a uniformly charged sphere of radius $r_C \times 10^{1/3}$ fm. The resulting potential parameters are given in Table I and the fits are plotted on Fig. 2 as the solid and dashed curves for $^{10}B + {}^{6}Li$ and $^{10}B + {}^{7}Li$, respectively. The agreement with the data is satisfactory, although some details of the experimental angular distributions could not be well reproduced, e.g., the peak in the $^{10}B + {}^{7}Li$ distribution at $\theta_{c.m.} \approx 40^\circ$ and its associated minimum. The corresponding total reaction cross sections (σ_R) are 1417 and 1490 mb for $^{10}B + {}^{6}Li$ and $^{10}B + {}^{7}Li$, respectively, reflecting the larger elastic scattering cross section at backward angles for $^{10}B + {}^{6}Li$, although the difference of only ≈5% in σ_R is much less marked than that between the angular distributions. The real potentials are very similar, that for ^{7}Li having a slightly larger rms radius, while the ^{7}Li imaginary potential is significantly deeper in the nuclear interior. However, the ^{6}Li imaginary potential is slightly more diffuse than the ^{7}Li one, and the two imaginary potentials are very similar in magnitude at radii $r \approx$ 8-10 fm, although this is not physically significant since a notch test similar to that of Ref. [9] found that the elastic cross section is not sensitive to the imaginary potential for radii greater than about 8 fm. Test calculations confirmed that the difference in the backward angle elastic scattering cross sections for the two systems is essentially expressed by the difference in the imaginary parts of the best-fit optical potentials, the greater absorption for $^{10}B + {}^{7}Li$ leading to the smaller cross section observed for this system, as would be expected.

Before attempting to establish the origin of this extra absorption in the $^{10}B + {}^{7}Li$ system, we first examine the influence of ^{10}B ground state reorientation, which should be similar for both systems.

B. Influence of ^{10}B ground state reorientation on the elastic scattering

The CC analysis of Ref. [1] found a significant effect from the ground state reorientation coupling of ^{10}B on the $^{10}B + {}^{7}Li$ elastic scattering, particularly at backward angles. The next step in the current analysis was therefore to include the ground state reorientation coupling of ^{10}B, common to both systems. The Coulomb coupling strength was derived from the measured ground state quadrupole moment [3] assuming the collective model. However, for such light systems Coulomb effects are relatively unimportant, so that the influence of the reorientation coupling on the elastic scattering will mainly depend on the choice of the nuclear coupling strength, which cannot be fixed directly by fitting data. We took a value of $\delta_2 = 1.8$ fm for the nuclear deformation length, as used in Ref. [1], obtained by fitting the $^{10}B + {}^{7}Li$ inelastic scattering data assuming the standard rotational model with $K = 1$. The nuclear form factor was of the standard derivative form, as employed in

TABLE I. Parameters of the optical model potentials used in the calculations. All the radii are defined as $R_i = r_i \times 10^{1/3}$ fm.

Set	V_0 [MeV]	r_V [fm]	a_V [fm]	W_0 [MeV]	r_W [fm]	a_W [fm]	r_C [fm]	Ref.
$^{10}B + {}^{6}Li$	161.4	1.274	0.709	6.59	2.348	0.970	1.30	This work[a]
$^{10}B + {}^{6}Li$	207.3	1.143	0.804	6.90	2.500	0.644	1.30	This work[b]
$^{10}B + {}^{7}Li$	167.2	1.312	0.669	8.08	2.478	0.871	1.30	This work[a]
$^{10}B + {}^{7}Li$	197.8	1.283	0.718	8.93	2.453	0.761	1.30	This work[b]
$^{10}B + {}^{7}Li$	221.0	1.174	0.758	10.1	2.288	0.820	1.30	This work[c]
$\alpha + {}^{10}B$	63.22	1.782	0.523	3.74	1.782	0.523	1.34	This work
$d + {}^{10}B$	78.0	0.921	0.943	30.0	0.867	0.731	1.30	[14]

[a]OM fit.
[b]CC fit, ^{10}B reorientation only.
[c]CC fit, $^{10}B + {}^{7}Li$ reorientation.

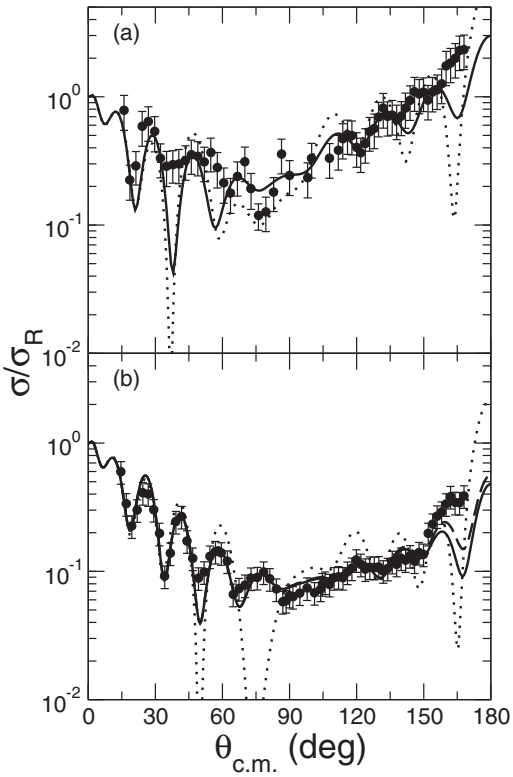

FIG. 3. (a) The present 51-MeV ^{10}B + ^{6}Li elastic scattering data (filled circles) compared to the result of a CC fit including ^{10}B ground state reorientation coupling (solid curve). The dotted curve denotes the effect of switching off the ^{10}B reorientation coupling. (b) The 51-MeV ^{10}B + ^{7}Li elastic scattering data of Rudchik *et al.* [1] (filled circles) compared to the result of a CC fit including ^{10}B ground state reorientation coupling (solid curve). The dotted curve denotes the effect of switching off the ^{10}B reorientation coupling. The dashed curve denotes the effect of including the ^{7}Li(^{10}B, ^{7}Li) ^{10}B elastic transfer coupling using the spectroscopic amplitudes of Ref. [1].

Ref. [1]:

$$F(r) = -\frac{\delta_2}{\sqrt{4\pi}}\frac{dU(r)}{dr}, \tag{1}$$

where $U(r)$ is the diagonal optical potential.

In Fig. 3, we plot as the solid curves the results of CC fits to the elastic scattering including the ^{10}B ground state reorientation coupling only. The parameters of the diagonal optical potentials were adjusted to obtain the best fits to the data when the reorientation couplings were included and the resulting values are given in Table I. The dotted curves denote the effect of switching off the reorientation coupling. The ^{10}B reorientation has an important influence on the elastic scattering for both systems and explicitly including this coupling enables a better description of both data sets than the simple optical model fits shown in Fig. 2. This is particularly noticeable for the ^{10}B + ^{7}Li data at angles $\theta_{\rm c.m.} \approx 40^\circ$. There is also a significant qualitative difference in the coupling effect in the two systems, most striking in the angular range $\theta_{\rm c.m.} = 60$–90°. The $\sigma_{\rm R}$ values are now 1253 and 1352 mb for ^{10}B + ^{6}Li and ^{10}B + ^{7}Li, respectively, a difference of ≈8%. This reflects the better fit to the data than was obtained by the OM calculations.

C. Influence of elastic transfer

The fits to both data sets exhibit a slight underprediction at angles $\theta_{\rm c.m.} > 150^\circ$ which we were unable to improve by searching on the bare optical potential parameters used in the CC calculations without significantly degrading the fit at smaller scattering angles. It is tempting to ascribe this to the influence of the ^{6}Li(^{10}B, ^{6}Li) ^{10}B and ^{7}Li(^{10}B, ^{7}Li) ^{10}B elastic transfer processes and in order to test this possibility CRC calculations were performed using the appropriate ^{4}He and ^{3}He spectroscopic amplitudes from Ref. [1]. The ^{4}He and ^{3}He clusters were bound to the ^{6}Li and ^{7}Li cores in Woods-Saxon potential wells with parameters taken from Ref. [1]. The ^{4}He elastic transfer had a negligible effect on the ^{10}B + ^{6}Li elastic scattering; the CRC angular distribution was indistinguishable from the CC result denoted by the solid curve in Fig. 3(a). However, the ^{3}He elastic transfer was able to account for some of the discrepancy between the CC calculation and the ^{10}B + ^{7}Li data at angles $\theta_{\rm c.m.} > 150^\circ$ without affecting the good description at more forward angles, cf. the dashed and solid curves in Fig. 3(b), but its influence on $\sigma_{\rm R}$ is negligible.

D. Influence of ^{7}Li ground state reorientation

Since the ground state quadrupole moment of ^{7}Li is also large [10], the effect of coupling to the ground state reorientation of this nucleus on the ^{10}B + ^{7}Li elastic scattering was also investigated. The calculations presented in Ref. [1] suggest that its influence is smaller than that of the ^{10}B ground state reorientation coupling. The Coulomb coupling strength was fixed using the measured ground state quadrupole moment [10] assuming a $K = 1/2$ collective model and the nuclear deformation length of 2 fm was taken from Ref. [1]. The result of a CC fit including both ^{7}Li and ^{10}B ground state reorientation couplings to the 51 MeV ^{10}B + ^{7}Li elastic scattering data of Ref. [1] is shown on Fig. 4 as the solid curve. The diagonal optical potential parameters were readjusted to recover the best fit to the elastic scattering data with the ^{7}Li ground state reorientation also included in the coupling scheme and the resulting values are given in Table I.

The quality of the fit to the data is not significantly altered by the inclusion of the ^{7}Li reorientation coupling but there are two things to note. First, the angular distribution produced by the bare, no-coupling calculation is now much closer to that for the ^{10}B + ^{6}Li system than was the case for the calculations including just the ^{10}B reorientation shown in Fig. 3. This is distinctly so over the angular range $\theta_{\rm c.m.} = 60$–90°. Second, the combined effect of the two reorientation couplings is smaller than their individual effects, suggesting some sort of interference effect. The $\sigma_{\rm R}$ value obtained from the calculation including both ^{10}B and ^{7}Li reorientation couplings is 1320 mb.

E. Summary of ground state reorientation and elastic transfer coupling effects

The results of the various CC and CRC calculations described above may be briefly summarized as follows. First,

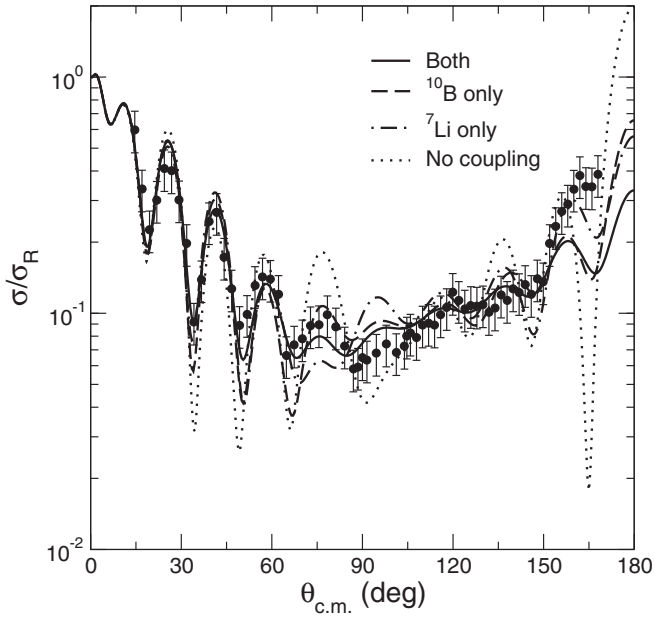

FIG. 4. The 51-MeV $^{10}B + ^{7}Li$ elastic scattering data of Rudchik *et al.* [1] (filled circles) compared to the result of a CC fit including both ^{7}Li and ^{10}B ground state reorientation couplings (solid curve). The dotted curve denotes the effect of switching off both couplings. The dashed and dot-dashed curves denote the separate effects of the ^{10}B and ^{7}Li reorientation couplings, respectively.

the significant difference between the 51-MeV $^{10}B + ^{6}Li$ and $^{10}B + ^{7}Li$ elastic scattering angular distributions at backward angles is not explained by the elastic transfer of ^{4}He and ^{3}He clusters between the ^{6}Li and ^{7}Li cores, respectively. On the contrary, the ^{4}He elastic transfer in the $^{10}B + ^{6}Li$ system has a negligible effect on the elastic scattering. The ^{3}He elastic transfer in the $^{10}B + ^{7}Li$ system does have a visible effect at angles $\theta_{c.m.} > 150^{\circ}$ but it is not significant. These results are consistent with the shell model spectroscopic amplitudes for these overlaps [1]. Second, while it might be expected that the effect of coupling to the ^{10}B ground state reorientation on the elastic scattering should be similar for both systems, a comparison of the solid and dotted curves on Figs. 3(a) and 3(b) indicates that there are significant qualitative and quantitative differences in the effect, particularly in the angular range $\theta_{c.m.} = 60$–90°. However, the bare potentials used in these calculations will not be the "true" ones since they were obtained by fitting the data with a very limited coupling scheme. Figure 4 shows that the inclusion of the ^{7}Li ground state reorientation coupling can account for a large part of the apparent difference but a significant fraction of it remains to be explained.

The explanation of these two questions should therefore lie in differences in the coupling effect of transfer and/or breakup channels between the two systems. Unfortunately, transfer data are not available for the $^{10}B + ^{6}Li$ system and, as was found in previous work [11], the coupling effects of transfer channels can strongly depend on the OM potential in the exit channel. Since OM potentials for most of the exit channels of interest are not available, without the requisite transfer data to fix the transfer strengths accurately, meaningful conclusions are not possible. We therefore concentrate on the influence of breakup couplings.

F. Breakup coupling effects

Since the experiment was performed in inverse kinematics, it allowed measurements of the differential cross section angular distributions for excitations of ^{6}Li to the $\alpha + d$ resonant states placed at excitation energies of 2.19, 4.31, and 5.65 MeV, i.e., the $^{6}Li \rightarrow \alpha + d$ resonant breakup cross sections, without the need for a complex coincidence experiment and its accompanying intricate data reduction procedure by detecting the scattered ^{10}B nuclei. However, this does limit the range of the resulting angular distributions to angles $\theta_{c.m.} < 120^{\circ}$. In addition, as explained earlier, the state at 2.19 MeV could not be resolved from the excitation of the 2.15-MeV state of ^{10}B. Similar data are available for excitation of the ^{7}Li 0.478-MeV $1/2^{-}$ bound excited state and 4.63-MeV $7/2^{-}$ and 6.68-MeV $5/2^{-}$ $^{7}Li \rightarrow \alpha + t$ resonant states [1]. These data enable the coupling strengths of the main breakup processes included in our calculations to be verified. The analyses for both systems were carried out using the well-established CDCC method.

We begin with a description of the calculations for the $^{10}B + ^{6}Li$ system. An $\alpha + d$ cluster structure was assumed for ^{6}Li [12], with the ground state wave function calculated using a Woods-Saxon (WS) binding potential with parameters $R = 1.9$ fm and $a = 0.65$ fm [13] (the depth was adjusted to give the correct binding energy). The three $T = 0$ $\alpha + d$ resonances above the breakup threshold ($I^{\pi} = 3^{+}$, 2^{+} and 1^{+}) were treated as momentum bins, with widths corresponding to 0.1, 2.0, and 3.0 MeV, respectively. Their $L = 2$ cluster wave functions were calculated with WS potentials of the same geometry as for the ground state but with depths adjusted so that the calculated energies of the resonances matched the empirical values. This approach generates values for the reduced transition probabilities $B(E2)$ between the ground and resonant states close to the measured ones.

The $\alpha + d$ continuum above the breakup threshold was truncated at a momentum of $k_{max} = 1$ fm^{-1}, equivalent to a maximum excitation energy of 17.2 MeV, and discretized into equally sized bins in momentum space of width $\Delta k = 0.125$ fm^{-1}. Relative angular momenta between the α and d clusters of $L = 0$, 1, 2, 3, and 4 were included together with all allowed couplings (including continuum-continuum couplings) up to a multipolarity of $\lambda = 4$. The binning scheme for $L = 2$ was modified where appropriate to avoid double counting in the presence of the resonant bins. This binning scheme gives essentially converged elastic scattering and resonant breakup angular distributions over the whole angular range, the addition of extra L values having only a small effect. The diagonal and all coupling potentials were calculated using the cluster-folding model and empirical $d + ^{10}B$ and $\alpha + ^{10}B$ OM potentials obtained by fitting data at energies of 11.8 [14] and 21 MeV [15], respectively. The parameter values are given in Table I.

The results of the CDCC calculations for the $^{10}B + ^{6}Li$ elastic scattering and for resonant breakup via the 3^{+}, 2^{+}, and 1^{+} $\alpha + d$ cluster states are compared with the relevant data

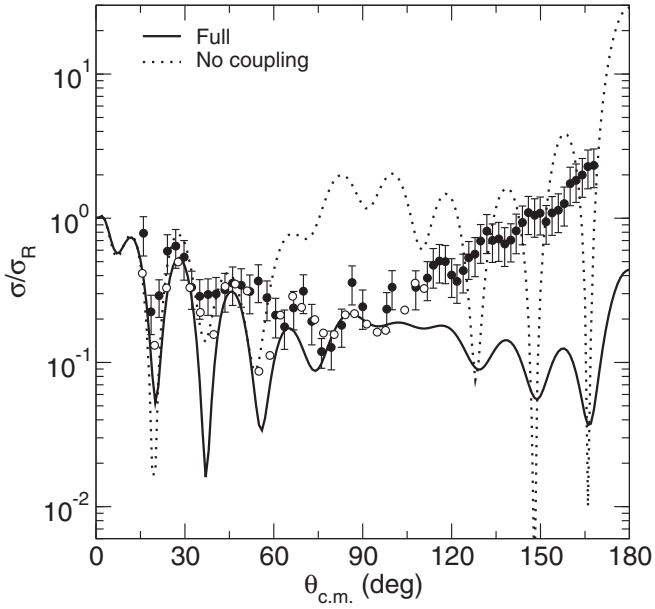

FIG. 5. Comparison of the results of CDCC calculations with the 51-MeV ^{10}B + ^{6}Li elastic scattering data. The filled circles denote the data obtained in this work and the open circles those of Kemper *et al.* [2]. The solid curve denotes the full calculation, including the nonresonant continuum, and the dotted curve the no-coupling result.

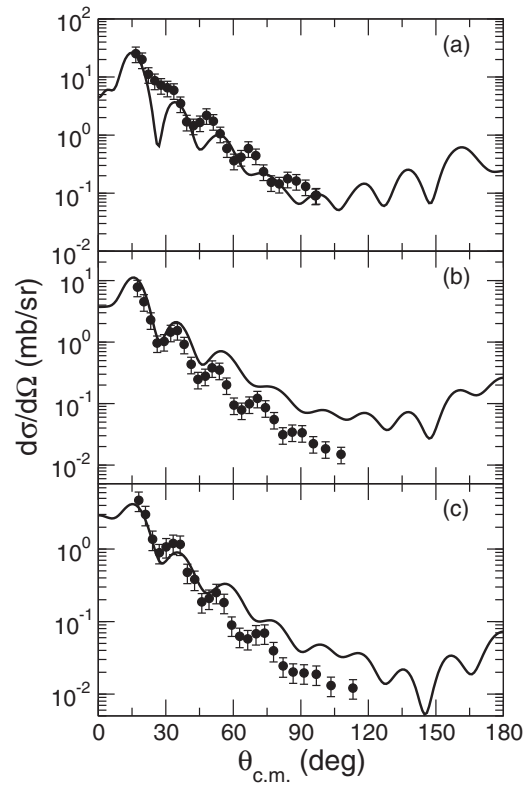

FIG. 6. Comparison of the results of CDCC calculations with the 51-MeV ^{10}B + ^{6}Li differential cross section data for ^{6}Li → $\alpha + d$ breakup via the three $L = 2$ resonant states of ^{6}Li: (a) the 2.19-MeV 3^+, (b) the 4.31-MeV 2^+, and (c) the 5.65-MeV 1^+. The solid curves denote the full calculation, including the nonresonant continuum. Note that the data in panel (a) represent the sum of the 2.19-MeV 3^+ ^{6}Li resonance and the unresolved 2.15-MeV 1^+ state of ^{10}B.

in Figs. 5 and 6. Note that the measured angular distribution in Fig. 6(a) represents the sum of the cross sections for excitation of the ^{6}Li 2.19-MeV 3^+ resonance and the unresolved ^{10}B 2.15-MeV 1^+ level. However, test calculations using the coupling parameters of Ref. [1] found that the contribution of the ^{10}B level is small, so may be safely neglected. The overall description of the elastic scattering data is reasonable, given that there are no adjustable parameters in the model used. Indeed, up to $\theta_{\text{c.m.}} \approx 115^\circ$ the description is rather good; at larger angles the data are significantly underpredicted by the calculation which is also more oscillatory. A comparison between the solid and dotted curves shows that the breakup coupling has a significant effect on the elastic scattering for angles $\theta_{\text{c.m.}} > 50^\circ$. Figure 6 shows that the general features of the angular distributions for resonant breakup via all three of the $L = 2$ resonant states are well described by the full CDCC calculation, although the details, such as the positions of maxima, are not always well reproduced. This is particularly so for the 2.19-MeV 3^+ resonance, Fig. 6(a). The data for breakup via the 4.31-MeV 2^+ and 5.65-MeV 1^+ are moderately overpredicted for angles $\theta_{\text{c.m.}} > 50^\circ$. Integrated cross sections extracted from the CDCC calculations are 13.05, 7.56, and 3.50 mb for resonant breakup via the 2.19-MeV 3^+, 4.31-MeV 2^+, and 5.65-MeV 1^+ levels, respectively.

We now describe the ^{10}B + ^{7}Li CDCC calculations. An $\alpha + t$ cluster structure was assumed for ^{7}Li, with a Gaussian binding potential taken from Ref. [16]. This model well reproduces the ground-state properties of ^{7}Li as well as the measured $B(E2)$ for excitation of the 0.478-MeV $1/2^-$ bound first excited state. The same "geometry" parameters were used for the ground, $1/2^-$ bound and 4.63-MeV $7/2^-$ and 6.68-MeV $5/2^-$ $L = 3$ resonant excited states, the depths being adjusted to give either the corresponding binding energy or a resonance at the appropriate excitation energy.

The $\alpha + t$ continuum was truncated at a momentum of $k_{\text{max}} = 1.0$ fm^{-1}, corresponding to an excitation energy of 14.7 MeV, and discretized into bins of width $\Delta k = 0.2$ fm^{-1}. Relative angular momenta of $L = 0$, 1, 2, 3, 4, and 5 between the $\alpha + t$ clusters were included, with all allowed couplings up to multipolarity $\lambda = 4$. This binning scheme was appropriately modified for $L = 3$ to avoid double counting in the presence of the $L = 3$ resonances. Full convergence was essentially obtained with this scheme; as for ^{6}Li, the addition of further L values to the continuum made only relatively small differences to the results. Diagonal and coupling potentials were again calculated using the cluster-folding model using the same α-particle OM potential as for ^{6}Li and the global t OM potential parameters of Ref. [17], specifically adapted to p-shell target nuclei.

The results of the CDCC calculations for the ^{10}B + ^{7}Li system are compared with the relevant data of Ref. [1] in Figs. 7 and 8. The overall description of the elastic scattering data by the full calculation is acceptable for angles $\theta_{\text{c.m.}} < 75^\circ$, given that there are no directly adjustable parameters in the CDCC calculation, and good for angles $\theta_{\text{c.m.}} < 60^\circ$. At

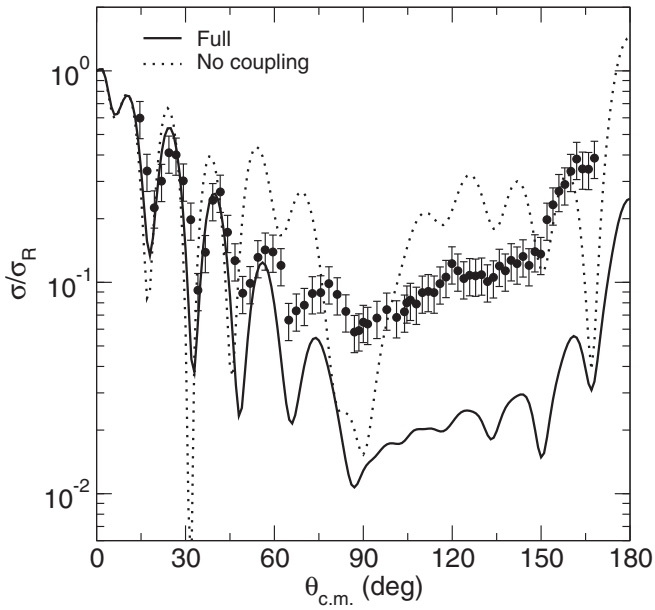

FIG. 7. Comparison of the results of CDCC calculations with the 51-MeV $^{10}B + {}^{7}Li$ elastic scattering data of Ref. [1] (filled circles). The solid curve denotes the full calculation, including the nonresonant continuum, and the dotted curve the no-coupling result.

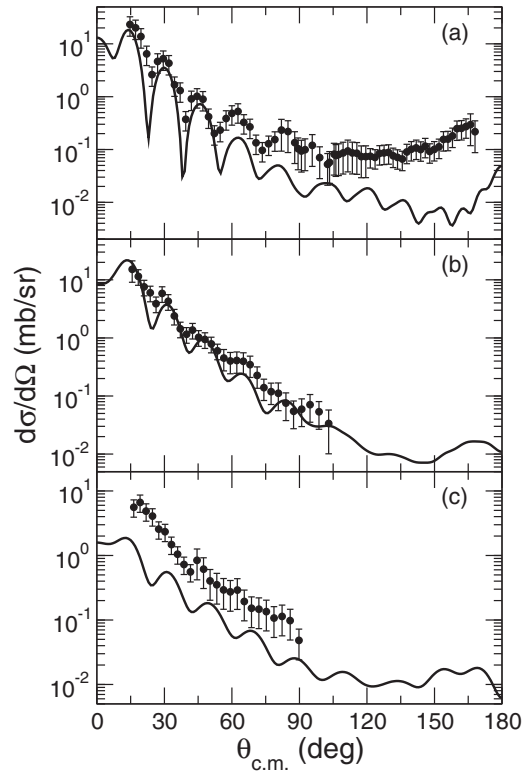

FIG. 8. Comparison of the results of CDCC calculations with the 51-MeV $^{10}B + {}^{7}Li$ differential cross section data for (a) excitation of the ^{7}Li 0.478-MeV $1/2^-$ bound excited state, (b) $^{7}Li \rightarrow \alpha + t$ breakup via the 4.63-MeV $7/2^-$ $L = 3$ resonant state, and (c) $^{7}Li \rightarrow \alpha + t$ breakup via the 6.68-MeV $5/2^-$ $L = 3$ resonant state. The solid curves denote the full calculation, including the nonresonant continuum, and the filled circles the data of Ref. [1].

larger angles, the calculation underpredicts the data by about an order of magnitude, although the general shape of the angular distribution is quite well reproduced. A comparison of the solid and dotted curves shows that the breakup coupling effect is significant for angles $\theta_{\text{c.m.}} > 45^\circ$ and is qualitatively similar to that for ^{6}Li, i.e., a general reduction of the cross section. However, the effect is stronger for ^{7}Li, despite the greater breakup threshold, although the more oscillatory nature of the ^{6}Li angular distributions makes this difficult to quantify accurately. The description of the data for excitation of the 0.478-MeV $1/2^-$ and 4.63-MeV $7/2^-$ states by the full CDCC calculation is good, with a slight underprediction of the $1/2^-$ data for angles $\theta_{\text{c.m.}} > 60^\circ$, presumably linked to the similar occurrence in the elastic scattering. However, the calculation underpredicts the data for excitation of the 6.68-MeV $5/2^-$ state by a factor of about three. Integrated cross sections extracted from the CDCC calculations are 6.66, 10.02, and 1.46 mb for population of the 0.478-MeV $1/2^-$, 4.63-MeV $7/2^-$, and 6.68-MeV $5/2^-$ states, respectively.

IV. SUMMARY AND CONCLUSIONS

A set of experimental data was obtained for the $^{10}B + {}^{6}Li$ system comprising angular distributions for the elastic scattering and resonant breakup via the three $L = 2$, $\alpha + d$ resonances of ^{6}Li in a experiment performed in inverse kinematics at the Heavy Ion Laboratory of the University of Warsaw, with a ^{10}B beam accelerated to 51 MeV. These data make possible a comparison with existing measurements for the $^{10}B + {}^{7}Li$ system at the same incident ^{10}B energy [1]. It is found that there are significant differences in the two elastic scattering angular distributions, not only in the phase of the oscillations at forward angles but also in the magnitude of the cross section at backward angles, that for $^{10}B + {}^{6}Li$ being significantly larger.

A natural inference is that the larger backward angle elastic scattering cross section for the $^{10}B + {}^{6}Li$ system could be due to the elastic transfer of a ^{4}He cluster between the two ^{6}Li cores; the $^{4}He + {}^{6}Li$ threshold of ^{10}B, 4.46 MeV, suggests that this process should be more favored than the corresponding ^{3}He elastic transfer in the $^{10}B + {}^{7}Li$ system since the $^{3}He + {}^{7}Li$ threshold is 17.79 MeV. However, CRC calculations using the TISM spectroscopic amplitudes of Ref. [1] found that the ^{4}He elastic transfer has a negligible effect on the $^{10}B + {}^{6}Li$ elastic scattering. Contrary to expectations, the ^{3}He elastic transfer has a visible effect on the $^{10}B + {}^{7}Li$ elastic scattering at angles $\theta_{\text{c.m.}} > 150^\circ$, although it is not significant. Our first conclusion is therefore that the larger backward-angle elastic scattering cross section for the $^{10}B + {}^{6}Li$ system compared to that for $^{10}B + {}^{7}Li$ cannot be accounted for by the elastic transfer process; the relevant ^{4}He spectroscopic amplitude would need to be almost an order of magnitude larger than the TISM value for the elastic transfer to have a significant impact on the $^{10}B + {}^{6}Li$ elastic scattering.

Coupled channel calculations confirmed the strong influence of the ^{10}B ground state reorientation coupling on the elastic scattering found in Ref. [1]. However, there were

significant qualitative and quantitative differences in the coupling effect for the two systems, particularly in the midangle range. Since the coupling effect of ^{10}B channels should be similar for both systems, it was conjectured that the differences are due to the extremely limited coupling scheme employed in these calculations—a single coupling—meaning that the bare, no-coupling potentials contain contributions simulating the effect of channels not included in the coupling scheme and are thus not the "true" bare potentials. Since one of the more important differences between ^{6}Li and ^{7}Li is the relatively large ground state quadrupole moment of ^{7}Li, whereas that of ^{6}Li is essentially zero, and since the ground state reorientation coupling for ^{7}Li is known to have a significant effect on the elastic scattering, a further CC fit to the $^{10}\mathrm{B} + ^{7}$Li elastic scattering data was obtained including the ^{7}Li reorientation as well as the ^{10}B. The ^{7}Li reorientation was able to account for a large part of the difference in the coupling effect seen in the CC fits including just the ^{10}B reorientation but by no means all of it. Perhaps more significantly, it did not account for any of the difference in magnitude of the backward angle elastic scattering cross section. It was also found that the combined influence of the ^{7}Li and ^{10}B reorientation couplings when included simultaneously seems to result from an interference effect of some kind.

It has thus been established that at least one of the nuclear structure differences between ^{6}Li and ^{7}Li, the fact that the ^{7}Li ground state is significantly deformed and thus exhibits an important reorientation coupling effect absent from ^{6}Li scattering, does not account for the difference in magnitude of the backward angle elastic scattering for the $^{10}\mathrm{B} + ^{6}$Li and $^{10}\mathrm{B} + ^{7}$Li systems. Furthermore, the ^{7}Li ground state reorientation interacts with the ^{10}B reorientation in a such a way that their combined coupling influence appears to be the result of a more-or-less complex interference between the two couplings.

Two possibilities remain to explain the difference in the backward angle elastic scattering between the two systems: either transfer couplings (other than the elastic transfer already investigated) or breakup couplings, since both will depend on the details of the nuclear structure of the different Li isotopes. Unfortunately, since data for the transfer reactions in the $^{10}\mathrm{B} + ^{6}$Li system are not available, so that the (unknown) OM potentials in the exit channels cannot be fixed by fitting the relevant data, a meaningful comparison of transfer effects between the two systems is not at present possible, previous work having found that coupling effects in light systems such as these can depend significantly on the choice of exit channel OM potential [11].

Breakup couplings can be adequately handled within the CDCC approach. However, due to the method by which CDCC is implemented within the code FRESCO it is not possible explicitly to include the ^{10}B reorientation coupling simultaneously with the Li breakup. Since this coupling was found to have a significant effect on the elastic scattering, the forced omission of this coupling could impact on the results of the CDCC calculations. However, the ^{10}B reorientation will have an indirect influence on the CDCC calculations via the use of empirical OM potentials for the ^{4}He, d, and $t + ^{10}$B elastic scattering used as input to the cluster-folding procedure generating the $^{10}\mathrm{B} + ^{6,7}$Li diagonal and coupling potentials used within the CDCC procedure. Since these potentials are fitted to data they will effectively simulate the gross effect of the ground state reorientation as well as that of the inelastic excitations of ^{10}B. There is a slight caveat for the $^{10}\mathrm{B} + ^{7}$Li case in that the apparent interference effects between the ^{7}Li and ^{10}B reorientation couplings will not be accounted for.

The CDCC calculations are able to provide a satisfactory overall description of the elastic scattering and resonant breakup data for the two systems, given that they contain no (directly) adjustable parameters. The exceptions are the $^{10}\mathrm{B} + ^{7}$Li elastic scattering at angles $\theta_{\mathrm{c.m.}} > 75^{\circ}$ and the resonant breakup via the 6.68-MeV $5/2^{-}$ resonance of ^{7}Li, which are poorly described. The first conclusion regarding the CDCC calculations concerns the apparent good agreement between the calculated and measured elastic scattering angular distributions for both systems at angles $\theta_{\mathrm{c.m.}} < 75^{\circ}$. This suggests that the use of empirical OM potentials fitted to the relevant ^{4}He, d, and $t + ^{10}$B elastic scattering data is able adequately to account for the bulk of the ^{10}B ground state reorientation coupling effect in this angular range, although some of the minima remain somewhat deeper than in the CC fits plotted on Fig. 3.

The greater breakup coupling effect at backward angles for $^{10}\mathrm{B} + ^{7}$Li compared to that for $^{10}\mathrm{B} + ^{6}$Li, plus the observation that this effect is to reduce the elastic scattering cross section for both systems, suggests that it could be a possible explanation for the significantly larger backward angle elastic scattering cross section in the $^{10}\mathrm{B} + ^{6}$Li system. However, there are two caveats to this conclusion: First, neither elastic scattering data set is well described by the CDCC calculations at backward angles. Second, while test $^{10}\mathrm{B} + ^{7}$Li calculations using a $t + ^{10}$B OM potential with a shallower real potential well yielding similar $t + ^{10}$B elastic scattering to the global potential of Ref. [17] gave a significantly better description of the backward angle $^{10}\mathrm{B} + ^{7}$Li elastic scattering, they exhibited a qualitatively different coupling effect. They were also considerably more numerically unstable, in that adequate convergence of the calculated backward angle elastic scattering as a function of the truncation in L of the $\alpha + t$ continuum could not be achieved. Thus, the question of whether the breakup coupling can account for the significant difference in the $^{10}\mathrm{B} + ^{6,7}$Li backward angle elastic scattering remains unproven.

The poor description of the resonant $^{7}\mathrm{Li} \rightarrow \alpha + t$ breakup via the 6.68-MeV $5/2^{-}$ level suggests either a greater sensitivity to the truncation of the nonresonant continuum model space or possibly a more complicated structure than the simple $\alpha + t$ cluster assumed in the model employed here. Tests found that the calculated angular distribution is largely insensitive to the truncation in L of the continuum model space, as are all the resonant breakup angular distributions for both systems, favoring the suggestion that this level may exhibit a more complicated structure than the 0.478-MeV $1/2^{-}$ and 4.63-MeV $7/2^{-}$ levels, both of which are well described by the CDCC calculation.

Finally, the question of the influence of couplings to transfer channels (other than the ^{4}He and ^{3}He elastic transfer) cannot be definitively answered without the relevant data for the $^{10}\mathrm{B} + ^{6}$Li system (such data already exist for $^{10}\mathrm{B} + ^{7}$Li

[1]) which are unfortunately not currently available. Previous experience with similar light systems (see, e.g., Ref. [11]) has shown that the transfer coupling influence can depend quite sensitively on the choice of exit channel OM potential parameters, which are unknown in this case, so that without the transfer data to help fix them reliable conclusions are impossible. Nevertheless, Ref. [11] showed that in the $^{6}Li + {}^{18}O$ system coupling to the $^{18}O(^{6}Li, {}^{7}Li)\,{}^{17}O$ single-neutron pickup alone could yield an increase of up to two orders of magnitude in the backward angle elastic scattering, *provided the backward angle transfer data were properly described by the calculation.* Thus, it is possible that similar effects could explain the difference between the $^{10}B + {}^{6}Li$ and $^{10}B + {}^{7}Li$ elastic scattering observed in this work.

In summary, the present work has highlighted some of the difficulties in unraveling the important reaction mechanisms in systems involving light heavy ions. There are many potential sources of strong coupling effects on the elastic scattering so that definitive answers to questions concerning the origin of important observed differences between the elastic scattering of similar systems at similar energies, as here, are seldom possible. However, the current state of direct reaction theory does to a large extent provide the necessary tools to give at least indications and suggest where additional data are required in order to go further.

ACKNOWLEDGMENT

This work was funded in part by the Polish National Agency for Academic Exchange (NAWA) within the Ulam Programme under Grant Agreement No. PPN/ULM/2019/1/00189/U/00001.

[1] A. T. Rudchik, V. O. Romanyshyn, E. I. Koshchy, A. Budzanowski, K. W. Kemper, K. Rusek, V. D. Chesnokova, J. Choiński, B. Czech, L. Głowacka, S. Kliczewski, V. M. Kyryanchuk, S. Y. Mezhevych, A. V. Mokhnach, O. A. Momotyuk, O. A. Ponkratenko, R. Siudak, I. Skwirczyńska, and A. Szczurek, Eur. Phys. J. A **33**, 317 (2007).

[2] K. W. Kemper, G. E. Moore, R. J. Puigh, and R. L. White, Phys. Rev. C **15**, 1726 (1977).

[3] P. Raghavan, At. Data Nucl. Data Tables **42**, 189 (1989).

[4] L. A. Parks, D. P. Stanley, L. H. Courtney, and K. W. Kemper, Phys. Rev. C **21**, 217 (1980).

[5] V. Hnizdo, K. W. Kemper, and J. Szymakowski, Phys. Rev. Lett. **46**, 590 (1981).

[6] J. Cederberg, D. Olson, J. Larson, G. Rakness, K. Jarausch, J. Schmidt, B. Borovsky, P. Larson, and B. Nelson, Phys. Rev. A **57**, 2539 (1998).

[7] M. Kowalczyk, SMAN: A Code for Nuclear Experiments, Warsaw University Report, 1998 (unpublished).

[8] I. J. Thompson, Comput. Phys. Rep. **7**, 167 (1988).

[9] F. Michel, J. Albinski, P. Belery, T. Delbar, G. Grégoire, B. Tasiaux, and G. Reidemeister, Phys. Rev. C **28**, 1904 (1983).

[10] A. Weller, P. Egelhof, R. Čaplar, O. Karban, D. Krämer, K.-H. Möbius, Z. Moroz, K. Rusek, E. Steffens, G. Tungate, K. Blatt, I. Koenig, and D. Fick, Phys. Rev. Lett. **55**, 480 (1985).

[11] K. Rusek, N. Keeley, K. W. Kemper, and A. T. Rudchik, Phys. Rev. C **91**, 044612 (2015).

[12] H. Nishioka, J. A. Tostevin, R. C. Johnson, and K.-I. Kubo, Nucl. Phys. A **415**, 230 (1984).

[13] K.-I. Kubo and M. Hirata, Nucl. Phys. A **187**, 186 (1972).

[14] W. Fitz, R. Jahr, and N. Santo, Nucl. Phys. A **101**, 449 (1967).

[15] P. David, J. Debrus, H. Mommsen, and A. Riccato, Nucl. Phys. A **182**, 234 (1972).

[16] B. Buck and A. C. Merchant, J. Phys. G **14**, L211 (1988).

[17] D. Y. Pang, W. M. Dean, and A. M. Mukhamedzhanov, Phys. Rev. C **91**, 024611 (2015).